J. Fluid Mech. (2018), *vol.* 851, *pp.* 1–22.
doi:10.1017/jfm.2018.460

Can a turbulent boundary layer become independent of the Reynolds number?

L. Djenidi[1,†], K. M. Talluru[2] and R. A. Antonia[1]

[1]School of Mechanical Engineering, University of Newcastle, Newcastle, NSW 2308, Australia

[2]School of Civil Engineering, The University of Sydney, Sydney, NSW 2006, Australia

(Received 19 November 2017; revised 27 April 2018; accepted 29 May 2018;
first published online 18 July 2018)

This paper examines the Reynolds number (Re) dependence of a zero-pressure-gradient (ZPG) turbulent boundary layer (TBL) which develops over a two-dimensional rough wall with a view to ascertaining whether this type of boundary layer can become independent of Re. Measurements are made using hot-wire anemometry over a rough wall that consists of a periodic arrangement of cylindrical rods with a streamwise spacing of eight times the rod diameter. The present results, together with those obtained over a sand-grain roughness at high Reynolds number, indicate that a Re-independent state can be achieved at a moderate Re. However, it is also found that the mean velocity distributions over different roughness geometries do not collapse when normalised by appropriate velocity and length scales. This lack of collapse is attributed to the difference in the drag coefficient between these geometries. We also show that the collapse of the U_τ-normalised mean velocity defect profiles may not necessarily reflect Re-independence. A better indicator of the asymptotic state of Re is the mean velocity defect profile normalised by the free-stream velocity and plotted as a function of y/δ, where y is the vertical distance from the wall and δ is the boundary layer thickness. This is well supported by the measurements.

Key words: turbulent boundary layers, turbulent flows

1. Introduction

The study of a turbulent boundary layer (hereafter denoted TBL) over a smooth wall at an ever increasing Reynolds number (Re) is motivated by the expectation that as Re increases, the boundary layer approaches an 'asymptotic' or Re-independent state. This would correspond to the ideal situation, where the viscous-dominated near-wall region is absent. Based on a self-preservation analysis (Townsend 1956, 1976), the mean velocity and Reynolds shear stress profiles can then be normalised using one velocity scale and one length scale. However, this asymptotic state of a smooth wall TBL is unlikely to be reached. First, it is impossible to achieve extremely high Re in a laboratory, thus preventing the possibility of investigating a Re-independent TBL, or a TBL with negligible viscous effects in the near-wall region (such that the viscous term in the equations of motion can be neglected in comparison

† Email address for correspondence: Lyazid.djenidi@newcastle.edu.au

to the other terms). Second, from an experimental point of view, if one increases *Re* to very large values, the TBL is unlikely to develop over a hydrodynamically smooth wall. This is because the thickness of viscosity-dominated near-wall layer decreases as *Re* increases. While no smooth wall TBL study has been carried out with an indefinitely increasing Reynolds number, it is expected that at some critical value of *Re*, this layer would become so thin that any imperfections of the surface would act as roughness. It should be noted that we are considering the case where *Re* is increased by increasing the free stream velocity and/or decreasing the kinematic viscosity. If one keeps these parameters constant and moves along the wall, *Re* increases but also the viscous scale. Consequently, a TBL over a nominally smooth wall will experience a continuous change in the wall roughness (inner-normalised roughness) as *Re* increases and will evolve from a smooth regime to a fully rough regime.

It is generally accepted (Hinze 1975) that for the fully rough regime, the effect of viscosity in the near-wall region becomes negligible (on a spatially averaged basis) and the coefficient of friction becomes independent of *Re*. This could present an interest if such a fully rough TBL can be interpreted as a surrogate to a smooth wall TBL with no viscous sublayer. Such a comparison may be possible if Townsend's wall similarity hypothesis or Townsend's Reynolds number similarity hypothesis (Townsend 1956, 1976) is valid. This hypothesis states that 'outside the viscous layer (region close to the surface) lies a region of fully turbulent flow, where the viscous stresses are small compared with the Reynolds stresses' and the outer flow is in a state of self-similarity. This outer region is thus thought to be nearly independent of viscosity of the fluid and determined by the wall shear stress and the channel width, pipe diameter or boundary layer thickness. Accordingly, if, at a moderate *Re*, the effect of viscosity in the near-wall region of the boundary layer is removed or made negligible on a spatially averaged basis (Talluru *et al.* 2016), then, according to the Reynolds number similarity, the boundary layer behaviour at that *Re* can be expected to be similar to that of a smooth wall boundary layer in the asymptotic state of *Re*.

There are numerous studies on rough wall flows reported in the literature which tested the validity of Townsend's hypothesis regarding the universal behaviour of the outer region of smooth and rough wall turbulent boundary layers. In the context of three-dimensional roughness, Flack, Schultz & Shapiro (2005), Volino, Schultz & Flack (2007), Squire *et al.* (2016) and references therein provide clear support to that hypothesis, at least when the ratio of roughness height (k) to boundary layer thickness (δ) is small. Similar observations are made in turbulent flows over two-dimensional roughness (Krogstad & Efros 2012, spanwise square bars) and three-dimensional roughness (Raupach 1981; Amir & Castro 2011). In contrast, there are other studies that reported differences in the outer layer region of smooth and rough wall flows (for example, Krogstad, Antonia & Browne 1992; Tachie, Bergstrom & Balachandar 2000; Leonardi *et al.* 2003; Bhaganagar, Kim & Coleman 2004; Lee & Sung 2007), raising a possible outer layer controversy as discussed by Antonia & Djenidi (2010). While this issue is not yet fully addressed, it is argued that the conflicting findings are often attributed to the large ratio k/δ (Jiménez 2004) used in some studies, wherein, a significant region of the boundary layer is directly influenced by the roughness. Jiménez (2004) suggests that there is a need for additional experiments in fully rough flows with large equivalent sand-grain roughness ($k_s^+ > 100$) and small relative roughness height ($\delta/k > 40$) in order to properly test Townsend's hypothesis. For a relatively recent account on wall-bounded turbulent flows over rough walls, the interested reader can consult Nickels (2010).

A common point that is conspicuously absent in all rough wall turbulent flow studies is a discussion on how different roughnesses can have different effects on the near-wall viscous region. In particular, it is not clear how the effects of viscosity in the near-wall region are altered (increased or dampened) by the roughness and how this alteration, which may be different for different roughness geometries, affects the flow dynamics. Further, there are no previous studies that report the effects of the removal (or weakening) of the near-wall viscosity-dominated layer on the development of the TBL and how such a TBL behaves with increasing *Re*. Thus, the novelty of the present study relates to the idea that by changing the boundary condition one can essentially get rid of the dampening effects of the viscosity in the near-wall region, which allows the boundary layer to grow faster than on a smooth wall, thus providing a method of 'simulating' high Reynolds number TBL, particularly in a low speed wind tunnel. Further, the ability to generate a TBL where the near-wall viscous effects are negligible, if not removed, provides the ideal conditions required to investigate Townsend's Reynolds number similarity hypothesis.

A practical and relatively simple method for removing or significantly reducing the viscosity effect in the near-wall region of a TBL at a moderate *Re* is to introduce roughness elements. In particular, a roughness consisting of transverse rods attached to the wall is quite effective for achieving a fully rough regime where the viscous drag is negligible or zero at relatively low *Re*. Leonardi *et al.* (2003) showed that a channel flow with a surface roughness made of periodic two-dimensional (2-D) transverse square bars has practically no (global) viscous drag when the spacing between two consecutive roughness elements is varied between 8 and 16 times the roughness height; the drag is almost entirely made up of form drag. Similar observations were made in the numerical simulation of a channel flow with 2-D circular rods as the roughness elements (Leonardi *et al.* 2015). In a recent experimental study, Kamruzzaman *et al.* (2015) measured the form drag directly using the static pressure distribution around a single circular rod on a 2-D rough wall (same as the current study) and found that the coefficient of friction becomes independent of *Re*. Similar results were reported by Bakken *et al.* (2005) in a rod-roughened turbulent channel flow. All these experimental and numerical results indicate that the spatially averaged viscous friction becomes zero, or at least negligible in comparison to form drag. In other words, the flow becomes fully rough. Interestingly, the *Re*-independence of the friction coefficient (C_f) is consistent with the Reynolds number similarity hypothesis and suggests that this hypothesis can be satisfied everywhere within a self-preserving turbulent boundary layer for which C_f is constant. This possibility is investigated here.

The present paper reports measurements made in a TBL which develops over a rough wall. The aim of the study is to assess the behaviour of the (rough wall) TBL as *Re* increases with the view to determining whether a *Re*-independent state can be achieved at a moderate *Re*. This objective is of great interest from both fundamental and practical viewpoints because it should help to address the following issues:

(i) Is there a universal asymptotic or *Re*-independent state for a TBL? If so, does this lead to a collapse of all normalised mean velocity profiles, for example?
(ii) Is the Reynolds number similarity valid or possible at moderate Reynolds numbers?
(iii) Can a fully rough wall TBL be used as a surrogate to a smooth wall TBL at extremely large *Re*.
(iv) What is the dynamical behaviour of an asymptotic TBL?

Evidently, care has to be exercised when extrapolating results obtained in a rough wall TBL at moderate Re to a smooth wall TBL in the asymptotic state of Re. Indeed, the physical mechanism which helps remove the effect of viscosity in the near-wall region of a rough wall TBL is most likely different to that over a smooth wall when the state of Re-independency is achieved. Issue (i) has an important implication for the prediction/estimation of some quantities. Indeed, the existence of a universal state can be exploited for developing models, such as the Clauser chart to estimate the friction coefficient, or the spectral chart developed by Djenidi & Antonia (2012) for estimating the turbulent kinetic energy dissipation rate. Issue (iv) is relevant for TBL control; in this context, it is important to ascertain how a Re-independent TBL responds to perturbations, e.g. wall suction, wall blowing, large eddy break up devices (LEBUs), wall roughness and whether a control strategy can be Re independent.

Finally, the idea that different asymptotic states may be associated with different boundary and/or initial conditions is not new. For example, George (1989) discussed the effect of initial conditions and coherent structures on the self-preservation states in various turbulent free shear flows (e.g. jets, wakes). Krogstad & Antonia (1999) discussed the effects of surface roughness on a TBL by comparing measurements from two different rough surfaces (a woven stainless steel mesh screen and transverse rods) with measurements in a smooth wall TBL ($Re_\theta = 12\,570$). Unfortunately, only one Reynolds number was considered in each case ($Re_\theta = 12\,800$ for the mesh screen surface, 4806 for the rod-roughened wall and 12 570 for the smooth wall; Re_θ is the Reynolds number based on the momentum thickness). Also, no study has been reported, where the roughness geometry and the Reynolds number are systematically varied. The present study, which complements and extends the investigation begun by Krogstad & Antonia (1999), is aimed at filling this knowledge gap.

2. Experimental details

Experiments are conducted in a boundary layer wind tunnel which was described in detail in Krogstad *et al.* (1992) and Kamruzzaman *et al.* (2015). Only the main features of the test section are described here. The test section is 5.4 m long and 0.9 m wide. At the exit of the contraction (6 : 1), the test section has a height of 0.15 m. It is tripped at the contraction exit by a 4 mm diameter rod followed by 170 mm long strip of No. 40 grit sandpaper. Following the contraction, the roof of the test section is adjusted in order to compensate for the growth of the boundary layers and to maintain a zero pressure gradient along the entire working section of the wind tunnel. The pressure gradient is maintained to be within $\pm 0.1\,\%$ of the free-stream dynamic pressure. The boundary layer develops over a rough wall, which consists of a periodic arrangement of cylindrical rods mounted on the wall and spanning across the full width of the test section (see figure 1). The diameter (k) of the rods is nominally 1.6 mm and the spacing (p) between the rods is set to $p/k = 8$. In all the experiments, the friction velocity (U_τ) is obtained by integrating the pressure distribution around the roughness element (see Kamruzzaman *et al.* 2015, for full details). For the virtual origin (d_0), we adopted the methodology put forth by Jackson (1981), who associated d_0 (as measured from the base of roughness) with the centroid of moments of forces acting on the roughness elements. Following this approach, moments were computed using the static pressure information around a single roughness element which resulted in a value of $d_0/k \approx 0.48$ for the present study. This is found to be consistent with the value of d_0/k reported in the numerical studies of Leonardi *et al.* (2003) and Lee & Sung (2007).

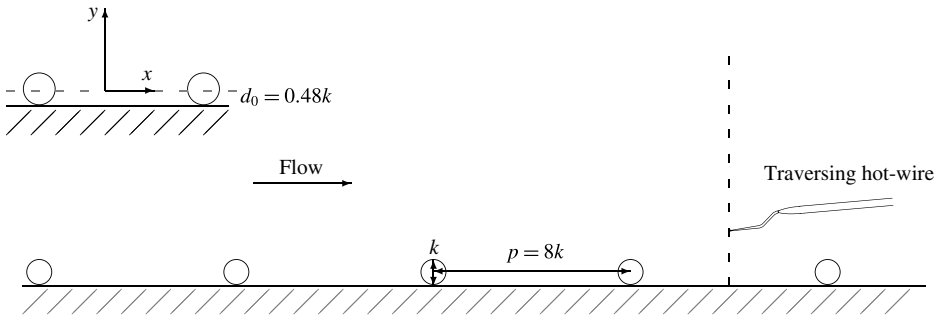

FIGURE 1. A schematic of the experimental set-up used in this investigation. The inset shows the coordinate system and the displacement height d_0.

x (m)	Sym.	Re_τ	Re_θ	U_∞ (m s^{-1})	ν/U_τ (μm)	U_τ (m s^{-1})	δ_{99} (m)	δ^* (m)	θ (m)	l^+	k_s^+	δ/k	δ/k_s	ΔU^+
Fixed x														
2.54	○	629	1 760	2.07	142	0.108	0.089	0.022	0.013	3.5	47	56	13.4	5.7
2.54	◇	1020	2 750	3.03	92.8	0.166	0.094	0.024	0.014	5.4	103	59	9.9	7.7
2.54	△	1516	3 922	4.17	64.6	0.238	0.098	0.026	0.015	7.7	220	61	6.9	9.6
2.54	□	2340	6 045	6.43	41.0	0.381	0.096	0.026	0.015	12.2	299	62	7.8	10.4
2.54	▷	3945	9 925	10.40	25.1	0.623	0.099	0.026	0.015	19.8	450	62	8.7	11.5
2.54	◁	5766	14 305	15.00	17.4	0.900	0.100	0.025	0.015	28.7	625	63	9.2	12.3
2.54	▽	7170	17 780	18.80	14.0	1.127	0.101	0.025	0.015	35.6	767	63	9.3	12.8
Different x														
1.94	●	5130	12 870	16.11	16.0	0.966	0.082	0.022	0.012	31	650	52	7.9	12.4
2.24	◆	5652	13 810	16.02	16.2	0.961	0.091	0.023	0.013	30.8	651	57	8.7	12.4
2.54	▲	6250	15 130	15.90	16.2	0.948	0.102	0.025	0.015	30.6	651	63	9.6	12.4
2.84	■	6588	15 880	15.57	16.6	0.934	0.109	0.026	0.016	30.1	651	68	10.1	12.4
3.14	▼	7140	16 310	15.85	16.2	0.951	0.116	0.026	0.016	30.7	651	73	10.9	12.4

TABLE 1. Experimental parameters over the 2-D rough wall. Note that the open symbols refer to data at a fixed location while the filled symbols represent data at different streamwise locations.

Two sets of experiments are carried out. For the first, measurements are made at 2.54 m downstream of the tripped inlet of the working section. The free-stream velocity, U_∞, is varied between 2 and 19 m s^{-1}. The boundary layer thickness (δ_{99}), is found to be nominally 0.1 m (approximately 63k). The Kármán Reynolds number, $Re_\tau = \delta_{99}U_\tau/\nu = \delta_{99}^+$ (where ν is the kinematic viscosity) ranges between 620 and 7200. For the second set of experiments, measurements are made at five streamwise locations between $x = 1.94$ and $x = 3.14$ m at $U_\infty \simeq 16$ m s^{-1}. The boundary layer properties for both sets of experiments are summarised in table 1, where δ^* and θ represent the displacement and momentum thicknesses, respectively. Throughout this paper, x and y refer to the streamwise and wall-normal directions, while u denotes the streamwise fluctuating velocity component. Further, (+) represents normalisation using viscous scales, for instance, $l^+ = lU_\tau/\nu$ and $U^+ = U/U_\tau$.

Note that all the measurements are taken at the mid-point of two adjacently spaced roughness elements, as shown by the vertical dashed line in figure 1. The near-wall part of the 'local' mean velocity profile varies with x, particularly in the region within and between two adjacent roughness elements. However, it was verified that the normalised velocity profiles measured at different longitudinal locations but with the same relative position with respect to the roughness elements collapsed onto a single profile. Thus, if one considers only the time-averaged equations of motion, it will result in x-dependence of mean momentum equation in the near-wall region. But, if one considers the double-averaged equations with respect to time and x as elaborated in Finnigan (2000), then the local x-variation (between the roughness elements) is eliminated.

Results from the present rough wall experiments are compared, when possible, with the smooth wall measurements of Marusic *et al.* (2015), the rough wall data of Squire *et al.* (2016) and the 2-D rough wall data of Krogstad & Efros (2012). The smooth wall measurements are performed using hot-wire anemometry in the large Melbourne boundary layer wind tunnel over a streamwise distance, $3.75 \leqslant x \leqslant 18$ m (Marusic *et al.* 2015). The Reynolds number at these measurement stations ranges between $3370 \leqslant \delta_{99}^{+} \leqslant 9830$. In all the smooth wall measurements, the friction velocity, U_τ, is obtained by fitting the logarithmic mean velocity profile to the constants $\kappa = 0.384$ and $B = 4.17$ (Chauhan, Nagib & Monkewitz 2009). For the rough wall measurements of Squire *et al.* (2016), only measurements at $x = 21.7$ m at different free-stream velocities are considered here. The primary reason for this is that Squire *et al.* (2016) measured U_τ at this particular streamwise location using a large drag balance, as described in Baars *et al.* (2016). This enables us to compare our results with those of Squire *et al.* (2016) without any ambiguity about U_τ. The 2-D rough wall measurements of Krogstad & Efros (2012) were made with using laser Doppler velocimetry (LDV) on a rough wall consisting of spanwise square bars (cross-section of 1.7 mm $\times$ 1.7 mm) arranged periodically with a spacing of $p/k = 8$, similar to the present study. A floating element balance was used to determine U_τ (see Krogstad & Efros 2010, for full details). The Kármán Reynolds number (δ^{+}) at $x = 6.2$ m on this rough wall is approximately 13 300 and k_s^{+} is approximately 320, suggesting that the flow is fully rough since $k_s^{+} \geqslant 100$ (Jiménez 2004).

2.1. *Hot-wire anemometry*

Hot-wire anemometry is used to measure streamwise velocity fluctuations. The single-wire probe is a Dantec 55P15 sensor; a 2.5 μm diameter Wollaston Pt -10%Rh wire is soldered between the prongs (separated by of 1.5 mm). The etched sensor length of the hot-wire is 0.5 mm giving a length to diameter ratio of 200, in keeping with the recommendations of Ligrani & Bradshaw (1987) and Hutchins *et al.* (2009). The inner-normalised sensor length (l^{+}) in these experiments varied between 3.5 and 35.6. The single-wire probe is operated using an in-house constant temperature anemometer at an overheat ratio of 1.8. A y-axis measuring device with a resolution of 1 μm is used in positioning the hot-wire probe close to the wall. The instrument comprises of a high magnification microscope 200$\times$ (Celestron digital microscope) mounted on a fine threaded traversing system. The measurement is accomplished using a digital indicator with a resolution of 0.001 mm. The indicator is set and zeroed on the top of the microscope and the displacement is recorded as the focusing is done from the wall to the hot-wire probe. A total of 36 logarithmically spaced measurement points between 0.2 and 136 mm are taken using the Mitutoyo height gauge with a resolution of 0.01 mm.

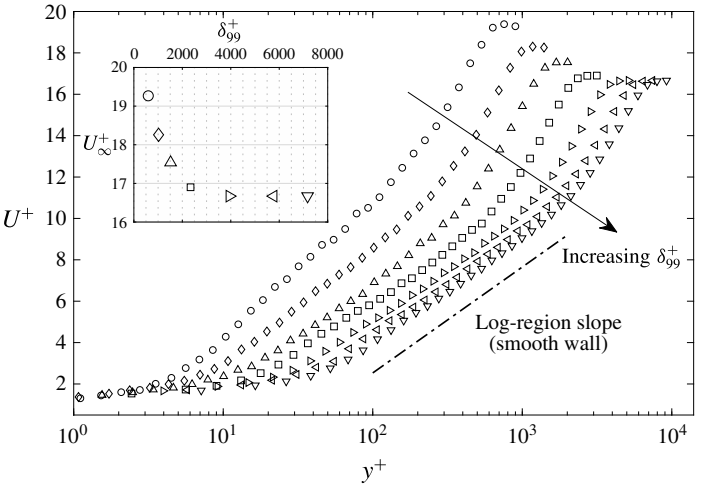

FIGURE 2. Present rough wall mean velocity profiles at several Reynolds numbers, $630 \leqslant \delta_{99}^+ \leqslant 7200$. See table 1 for symbols. The dot-dashed line represents the slope of the log region in a smooth wall turbulent boundary layer. Inset: variation of U_∞^+ with δ_{99}^+ (open symbols represent the corresponding δ^+ values).

A BAT-10 thermocouple (Physitemp) with a resolution of 0.1 °C was used to monitor the mean temperature in the free stream for the entire duration of the experiment. The hot-wire is calibrated *in situ* against the Pitot-static tube positioned in the undisturbed free-stream flow before and after every experiment at 16 different speeds ranging between 0 and 22 m s^{-1}. A linear interpolation in time between pre- and post-calibrations (see Talluru *et al.* 2014, for details) is used to account for any drift in the hot-wire voltage that occurs during the course of an experiment.

3. Results

3.1. *Mean velocity*

Figure 2 shows mean velocity profiles normalised using inner scaling parameters, i.e. U^+ versus y^+, at a fixed x location as $Re_\tau = \delta_{99}^+$ increases from 630 to 7200. It is clearly evident that the mean velocity profile shifts downward and towards larger y^+ as Re_τ increases, which is due to U_τ increasing with Re_τ. However, the rate of the downward shift decreases and eventually becomes zero, i.e. the mean velocity profile ceases to move downwards once Re_τ reaches a value of approximately 4000. Beyond this value, the profile simply shifts to larger y^+, while its shape remains unchanged. The inset plot in figure 2 shows the variation of U_∞^+ as a function of Re_τ (or δ_{99}^+). The trend is clear: as Re_τ increases, $U_\infty^+ (\equiv [\sqrt{C_f/2}]^{-1})$ first decreases before reaching a constant value for $Re_\tau \geqslant 4000$. This indicates that the downward shift ceases at the same time as the coefficient of friction becomes constant and the TBL can be considered fully rough; in this fully rough regime, the drag is solely made of the form drag of the roughness elements. The continuous shift of the entire profile to larger values of y^+ suggests that the length scale ν/U_τ is not an appropriate length scale. The profile continues to shift horizontally because U_τ increases with Re_τ (see table 1), thus resulting in y^+ increasing for a fixed value of y, but maintaining its shape.

To verify the fixed form of the shape, we plot in figure 3 the three velocity profiles in figure 2 for which U_∞^+ is constant as a function of y/k. There is a clear collapse

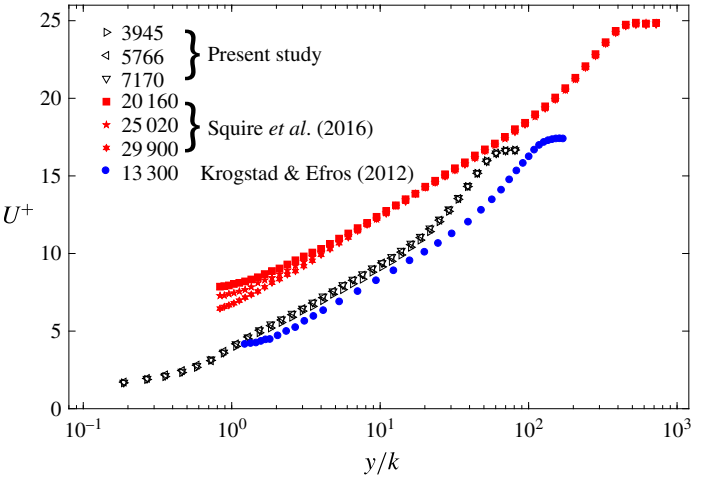

FIGURE 3. (Colour online) Mean velocity profiles in the present rough wall (black symbols) at several Reynolds numbers, $3940 \leqslant Re_\tau \leqslant 7200$, sand-grain roughness (red symbols, $Re_\tau = 20\,160$, $25\,020$ and $29\,900$, Squire *et al.* 2016) and square bar roughness (blue symbols, $Re_\tau = 13\,300$, Krogstad & Efros 2012) as a function of y/k.

of the profiles across the entire boundary layer onto a single curve of the form:

$$U^+ = F(y/k), \tag{3.1}$$

where F is a function, which appears to be independent of Reynolds number. A similar behaviour ($U^+_\infty = \text{const}$) can be observed in the sand-grain rough wall profiles of Squire *et al.* (2016) ($3970 \leqslant Re_\tau \leqslant 29\,900$). However, it is achieved at a much higher Re_τ than in the present rough wall, illustrating the fact that a sand-grain rough wall TBL requires a larger Re_τ than a 2-D rod rough wall TBL before it can become fully rough. For comparison, we also report in figure 3, the rough wall mean velocity profile of Krogstad & Efros (2012) (2-D transverse square bars with $p = 8k$). Considering that $\delta^+ = 13\,300$ and $k_s \simeq 325$, one expects the profile to be in the fully rough regime. Despite the large difference in Re_τ between our data and those of Krogstad & Efros (2012), the latter profile is not too different from the present distributions, although its value of U^+_{max} is slightly larger, reflecting a lower C_f in comparison to the present study; $C_f \simeq 0.0072$, and 0.0068, for the present 2-D rough wall and that of Krogstad & Efros (2012), respectively.

Figure 4 shows a clear collapse of the mean velocity profiles over the present rough wall, when plotted as a function of y/δ_{99}. The same trend is observed in the sand-grain roughness data of Squire *et al.* (2016), however, the latter collapse onto a different curve. This difference is due to the difference in C_f between the two rough wall TBLs. It is well known that there is no such collapse for smooth wall TBL profiles because of Re_τ-dependence of C_f. This is well illustrated in figure 4, where we plot the high Reynolds number smooth wall data of Marusic *et al.* (2015) ($3370 \leqslant Re_\tau \leqslant 9830$) and the direct numerical simulation (DNS) data of Schlatter & Örlü (2010) ($Re_\tau = 674$). Of particular interest, is the rough wall velocity profile of Krogstad & Efros (2012), also reported in the figure for comparison. This profile collapses relatively well onto the present 2-D rough wall profiles, as it could have been anticipated from figure 3 and the similar values of C_f, suggesting that both TBLs share similarities. This may

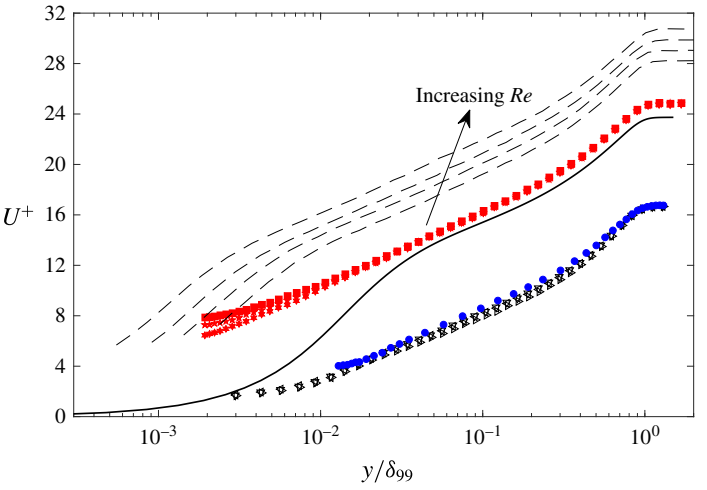

FIGURE 4. (Colour online) Mean velocity profiles over the present 2-D rough wall (back symbols) as a function of y/δ. Symbols as in table 1. Red symbols: (Squire *et al.* 2016, $Re_\tau = 20\,160$, 25 020, and 29 900); blue symbols: (Krogstad & Efros 2012, $Re_\tau = 13\,300$); dashed lines: smooth wall data (Marusic *et al.* 2015, $Re_\tau = 3370$, 4760, 6450 and 9830) and solid line: smooth wall DNS data (Schlatter & Örlü 2010, $Re_\tau = 674$). Only the profiles for which U_∞/U_τ is constant in the present rough wall and sand-grain roughness (Squire *et al.* 2016) TBLs are shown.

not be too surprising considering the rough walls share almost the same roughness geometry, cylindrical rods and square bars with the same k and p, although δ/k for the square bar rough wall is approximately twice the present value.

Altogether, the results presented in figures 2–4 are consistent with a *Re* independence of the normalised mean velocity profile, which would suggest that the Reynolds number similarity is well achieved in a rough wall TBL, at least in the context of the mean velocity. Note that unlike a smooth wall TBL, where one must exclude the viscous-dominated near-wall region if such similarity is to be observed, the Reynolds number similarity is observed across practically the entire boundary layer for a fully rough TBL. This is possible because the spatially averaged viscosity effects in the near-wall region are either zero or negligible. The sand-grain rough wall data of Squire *et al.* (2016) also show that when *Re* is large enough the normalised velocity profiles collapse onto a single distribution. However, that distribution differs from that of the present data due to a difference in the value of the form drag coefficient. To illustrate this, we employ the so-called diagnostic plot (Alfredsson 2010; Alfredsson, Segalini & Örlü 2011; Örlü *et al.* 2016), which consists of plotting u' as a function of U, thus removing any ambiguity associated with knowing y and U_τ accurately. Figure 5 shows such plots, where u' and U are normalised by U and U_∞, respectively. While for each surface there is a clear collapse of the distributions across the entire boundary layer, the collapse is different between the two surfaces, in conformity with two distinct drag coefficients ($C_f \simeq 0.0072$ and 0.0032 for the present data and the sand-grain roughness, respectively). Further, the trend shown by the data indicates that the distributions for the two rough walls will remain distinct, regardless of the Reynolds number, hence suggesting two distinct *Re*-independent profiles. It appears thus that a *Re*-independent normalised mean velocity profile for the complete TBL

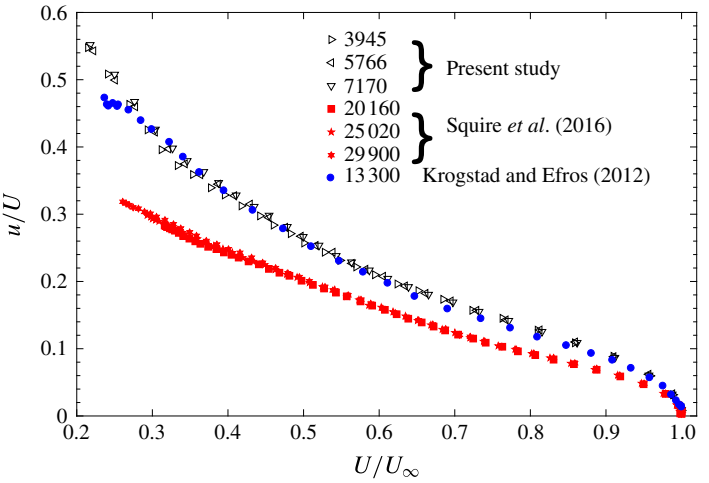

FIGURE 5. (Colour online) Diagnostic plot for the present rough wall (black symbols), sand-grain roughness (red symbols, $Re_\tau = 20\,160$, $25\,020$, and $29\,900$, Squire *et al.* 2016) and the square bar roughness (blue symbols, $Re_\tau = 13\,300$, Krogstad & Efros 2012).

is possible for fully rough wall TBLs. However, the profile cannot be universal since it is controlled by the rough wall drag coefficient which varies between roughness geometries as evidenced in figure 4.

Another parameter that is also likely to control the *Re*-independent profile of a rough wall TBL, for a given roughness geometry, is the ratio δ/k. It is expected that for a given roughness geometry, C_f will change with δ/k; $\delta/k = 63$ and 200 for the present profiles and those of Squire *et al.* (2016), respectively, shown in figures 4 and 5. This raises the following question: can the *Re*-independent profiles for both rough walls collapse if one varies δ/k? (Such collapse would result in both rough walls yielding the same diagnostic distribution.) The above results show that simply invoking Townsend's Reynolds number similarity to address the question is not enough. The answer requires one to carry out a series of parametric measurements for both rough wall TBLs in the fully rough regime by systematically changing the value of δ/k. However, one expects to observe the same result as presented here. Indeed, consider for example the 2-D rough wall where one changes k, while maintaining p/k constant and equal to 8. Regardless of k and as long as δ/k is large enough (at least larger than 40 (Jiménez 2004)), the fully rough regime will yield the same C_f as for the present case, and thus the same normalised velocity profiles as shown in figure 2 will be obtained. This appears to be confirmed by the data of Krogstad & Efros (2012) reported in figure 5. Despite the difference in the cross-sectional shape between the present roughness and that of Krogstad & Efros (2012) (circular rods versus square bars), the distributions are practically identical. Of course, the critical *Re* at which the fully rough regime will be achieved will vary with k. This implies that two distinct roughness geometries, as for example in the present work, will lead to two distinct *Re*-independent normalised mean velocity profiles in the fully rough regime. These differences can be further elucidated by comparing the turbulence intensity profiles in the outer region of the smooth and rough wall TBLs based on a modified diagnostic plot proposed by Castro, Segalini & Alfredsson (2013) and reported in figure 6. This modified diagnostic plot produces a better collapse of all

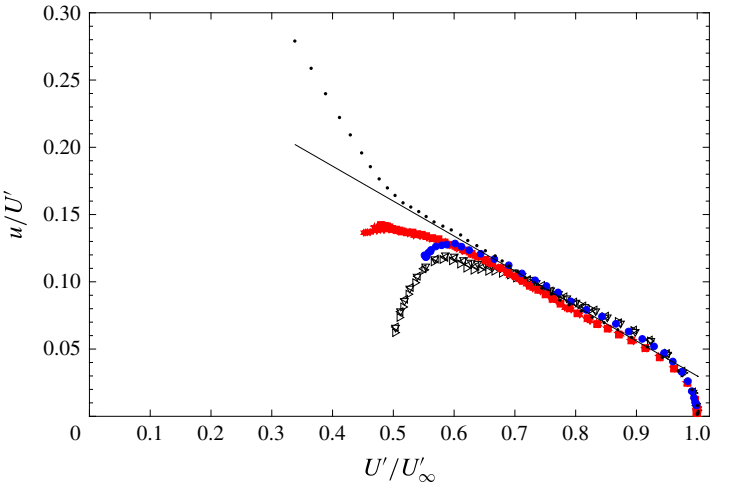

FIGURE 6. (Colour online) Comparison of turbulence intensities in the outer layer of smooth (dotted line, $Re_\tau = 9830$, Marusic *et al.* 2015) and rough wall turbulent boundary layers (data from figure 5) using the modified diagnostic plot (Castro *et al.* 2013). Here, $U' = U + \Delta U$ and $U'_\infty = U_\infty + \Delta U$ and ΔU is the velocity defect. The solid line is the smooth wall outer layer straight line from Alfredsson, Örlü & Segalini (2012).

curves than the original one. It seems that by introducing the velocity deficit (ΔU), the difference between smooth, and different types of rough walls is dramatically reduced. Note though that the collapse is not perfect. While the non-collapse for $U'/U'_\infty \leqslant 0.7$ can be explained in terms of the differences in turbulence levels in the near-wall region of different types of TBLs, the reason for the variation in the region $U'/U'_\infty \geqslant 0.8$ between the 2-D bars and the sand-grain roughness is not clear; this may reflect a real difference associated with the roughness geometry or the possibility that the sand-grain paper data of Squire *et al.* (2016) are not fully rough (albeit C_f appears to be constant in the experimental data of Squire *et al.* (2016)).

It is common to test the universality of TBL velocity profiles by plotting the velocity profiles in the deficit form, (Townsend 1956):

$$\frac{U_\infty - U}{u_o} = f(y/\eta), \tag{3.2}$$

where u_o and η are velocity and length scales, respectively, and have been the subject of many investigations (i.e. Townsend (1976), George & Castillo (1997), Zagarola & Smits (1998), Jones, Nickels & Marusic (2008), Talluru *et al.* (2016)). Here, we use U_τ, U_∞ and δ because Talluru *et al.* (2016) showed that these are correct scaling variables for rough wall TBLs (use of the length scale $\delta^*[2/C_f]^{1/2}$ (Rotta 1962), where δ^* is the displacement thickness, does not change the results). Figure 7(*a*,*b*) shows the velocity defect profiles for the rough wall data and the same smooth wall data as reported in figure 4 normalised by U_τ and U_∞, respectively. Universality is thought to be reflected in the collapse of the normalised velocity defect profiles. For the rough wall data, the use of either U_τ or U_∞ as a scaling velocity results in a good collapse. In particular, the collapse is perfect for the profiles for which U^+_∞ is constant, confirming that a *Re*-independent normalised velocity distribution is achieved. The smooth wall data present an interesting paradox: the velocity defect profiles

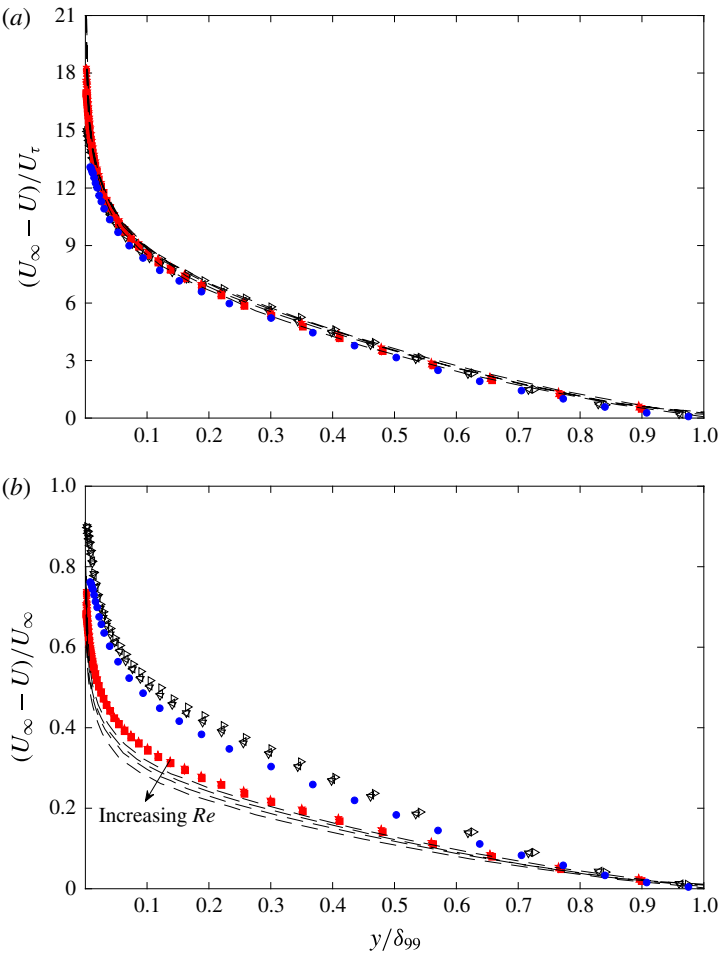

FIGURE 7. (Colour online) Comparison of velocity defect profiles in smooth wall (black dashed lines, $Re_\tau = 3370$, 4760, 6450 and 9830, Marusic *et al.* 2015), sand-grain roughness (red symbols, $Re_\tau = 20\,160$, 25 020 and 29 900, Squire *et al.* 2016), square bar (blue symbols, $Re_\tau = 13\,300$, Krogstad & Efros 2012) and the present rough wall data (black symbols) normalised by (*a*) U_τ and (*b*) U_∞. Refer to caption of figure 4 for symbols used for smooth wall, sand-grain and square bar rough wall TBLs.

collapse when normalised with U_τ, but not when normalised with U_∞. In order to solve this paradox we write the left-hand side of (3.2) as follows,

$$\frac{U_\infty - U}{U_\tau} = \left[\frac{2}{C_f}\right]^{1/2} \left(\frac{U_\infty - U}{U_\infty}\right). \tag{3.3}$$

For the smooth wall, C_f is function of Re; C_f decreases with increasing Re, thus compensating for the Re dependence of $(U_\infty - U)/U_\infty$ which leads to the collapse of the profiles. We note though that they collapse relatively well with the rough wall profiles when normalised with U_τ. The collapse of $(U_\infty - U)/U_\tau$ between the rough wall and the smooth wall data is often used to demonstrate the universality of the velocity profiles in TBLs and validate Townsend's Reynolds number similarity.

Interestingly, Townsend (1956) states that 'if, as must be assumed, Reynolds number similarity of self-preserving flow exists, the form of the self-preserving functions is universal for any one type of flow'. This implies that $(U_\infty - U)/U_\tau$ and $(U_\infty - U)/U_\infty$ must be similar in form for any Re, if both U_τ and U_∞ are proper scaling velocities compliant with self-preservation analysis (Talluru *et al.* 2016).

For the rough wall, C_f is constant in the fully rough regime. Thus, using either U_τ or U_∞ leads to the same collapse which is consistent with the Reynolds number similarity. The data of Squire *et al.* (2016) show the same result. Regardless of the choice of u_o, the normalised velocity defect profiles collapse. However, while the sand-grain rough wall data collapse with the present velocity defect profiles when normalised by U_τ, they collapse onto a different curve than the present rough wall one when normalised by U_∞. The data of Krogstad & Efros (2012) differ slightly from the present data when normalised by U_∞, certainly reflecting the slightly smaller value of C_f.

For the smooth wall, equation (3.3) indicates that $(U_\infty - U)/U_\tau$ and $(U_\infty - U)/U_\infty$ cannot both be Re-independent, as shown in figure 7(*a*,*b*), since C_f is Re-dependent. George & Castillo (1997) argued, based on the asymptotic invariance principle, that the velocity deficit in the outer layer scales as $(U_\infty - U)/U_\infty$ in the Re-independent regime. Note that even if the smooth wall profiles $(U_\infty - U)/U_\infty$ collapse (in the outer part of the layer); figure 7(*b*) shows that they will certainly collapse onto a different curve than that for the rough walls. Notice how the trend shown by the distributions altogether in figure 7(*b*) reflects that of the profiles in figure 4; as the distributions in figure 4 shift downwards, they shift upwards in figure 7(*b*). This can be explained if we write $1 - U/U_\infty = 1 - (U/U_\tau)(C_f/2)^{1/2}$. It appears then that $(U/U_\tau)(C_f/2)^{1/2}$ is larger for a smooth wall TBL than a rough wall TBL; further, while it is constant (i.e. independent of Re) for a given fully rough wall TBL, it increases with Re for a smooth wall TBL. This result shows that the distribution $(1 - U/U_\infty)$ or simply (U/U_∞) should be used for assessing a Re-independence state. Indeed, when such state is reached, the profiles, U/U_∞, must collapse onto a single curve; this curve varies with the roughness geometry or the coefficient of drag.

It is remarkable that while the profiles $(U_\infty - U)/U_\infty$ differ between smooth and rough walls, the profiles for $(U_\infty - U)/U_\tau$ collapse relatively well onto each other. We saw above that the compensational effect of C_f on $(U_\infty - U)/U_\infty$ leads to a collapse of the profiles $(U_\infty - U)/U_\tau$ for the smooth wall. However, the collapse of $(U_\infty - U)/U_\tau$ between the rough and smooth wall data may not in fact be too surprising. To see this, let us first note that the downward shift of the rough wall mean velocity profiles, ΔU^+, can be expressed across most of the boundary layer, as

$$\Delta U^+ = U^+_\infty|_{smooth} - U^+_\infty|_{rough} = \left(\frac{2}{C_f}\right)^{1/2}_{smooth} - \left(\frac{2}{C_f}\right)^{1/2}_{rough}. \tag{3.4}$$

We can then write

$$U^+_{smooth} = U^+_{rough} + \Delta U^+ = U^+_{rough} + \left(\frac{2}{C_f}\right)^{1/2}_{smooth} - \left(\frac{2}{C_f}\right)^{1/2}_{rough}. \tag{3.5}$$

Using (3.5), we can express the normalised defect profile $(U_\infty - U)/U_\tau$ as,

$$\left(\frac{U_\infty - U}{U_\tau}\right)_{smooth} = \left(\frac{2}{C_f}\right)^{1/2}_{smooth} - U^+_{rough} - \left(\frac{2}{C_f}\right)^{1/2}_{smooth} + \left(\frac{2}{C_f}\right)^{1/2}_{rough}. \tag{3.6}$$

Thus, we have

$$\left(\frac{U_\infty - U}{U_\tau}\right)_{smooth} = \left(\frac{U_\infty - U}{U_\tau}\right)_{rough}. \tag{3.7}$$

This explains the collapse of U_τ-normalised velocity defect profiles between rough wall and smooth wall TBLs. A similar equality can be established for velocity profiles over two different rough wall TBLs. Accordingly, one can expect that all smooth and rough wall (ZPG) TBL velocity defect profiles normalised by U_τ will collapse onto a single curve. Of course, equation (3.7) implies that the mean velocity (U^+) profiles in the rough wall TBLs are shifted downward by the same amount, ΔU^+, across most of the layer (e.g. $y/\delta_{99} \geqslant 0.1$) with respect to the smooth wall TBL profiles when δ_{99}^+ is the same for both TBLs. This seems a reasonable assumption according to figure 4 and the agreement observed in figure 7, which means that the rough wall mean velocity profiles are, apart from a downward shift, similar to the smooth wall mean velocity profiles. These results show that while the normalised mean velocity profiles do not collapse between different walls because of the change in drag coefficient, the shape of the distributions is the same. This is precisely Townsend's Reynolds number similarity applied to the outer region of TBLs. It is important to remember though that U_τ is not a scaling velocity compliant with self-preservation for the smooth wall TBL, at least for the outer part of the layer. This last remark should be discussed in the context of scaling of a ZPG TBL at a moderate Reynolds number. It can be shown (see, e.g. Townsend 1976; Talluru *et al.* 2016) for a ZPG TBL that the scaling velocity, u_o, which complies with self-preservation, must satisfy the following condition

$$\frac{u_o}{U_\infty} = C, \tag{3.8}$$

where C is a constant. We can write (3.8) as

$$u_o = CU_\infty = CU_\tau \left[\frac{2}{C_f}\right]^{1/2}. \tag{3.9}$$

For a fully rough ZPG TBL, where C_f is constant (independent of Re and x), both U_∞ and U_τ can be used as appropriate scaling velocities leading to normalised velocity profiles, to conform with self-preservation and Re-independence. For a smooth wall ZPG TBL, the use of $u_o = U_\infty$ (or $U_\tau[2/C_f]^{1/2}$) appears correct for a given U_∞, which implies that U_τ alone cannot be a scaling velocity since C_f is not constant (either with x or Re). Further, for a smooth wall, self-preservation (see Talluru *et al.* 2016) requires

$$\eta \sim \frac{\nu}{u_o}, \tag{3.10}$$

while u_o still obeys (3.9). Accordingly, we have

$$\eta \sim \frac{\nu}{U_\infty} = \frac{\nu}{U_\tau \left[\dfrac{2}{C_f}\right]^{1/2}}. \tag{3.11}$$

In the case of a fully rough wall TBL, this constraint does not exist since the viscous term in the mean equation of motion is removed (Talluru *et al.* 2016), thus discarding both ν/U_∞ and ν/U_τ as appropriate length scales. We already saw (figure 2) that ν/U_τ does not scale the velocity profiles. For a rough wall, since $U_\infty \sim U_\tau$ then ν/U_∞ cannot scale the velocity profiles either.

3.2. *Streamwise Reynolds normal stress*

The previous section strongly suggests that a rough wall TBL reaches a *Re*-independent state at a moderate *Re* in a fully rough regime in which the mean velocity profile remains unchanged when normalised by length and velocity which comply with self-preservation. It is then of interest to assess how the normalised Reynolds stresses, and in particular the streamwise Reynolds stress, behave as the rough wall TBL approaches its *Re*-independent state.

There is strong experimental evidence in the literature showing that the profile of $\overline{u^2}$ in a smooth wall TBL is considerably altered when *Re* increases (see Metzger *et al.* 2001; Hutchins & Marusic 2007; Marusic *et al.* 2010; Smits, McKeon & Marusic 2011, for example). This behaviour is illustrated in figure 8(*a*), which shows viscous-scale-normalised distributions of $\overline{u^2}$ in a smooth wall TBL as *Re* increases (DNS data of Schlatter & Örlü (2010), Re_τ = 674; wind tunnel measurements of Marusic *et al.* (2015), $3370 \leqslant Re_\tau \leqslant 9830$). At low Reynolds number, the turbulence intensity profile presents a characteristic peak at $y^+ \simeq 15$. Some relatively recent studies show that the near-wall peak exhibits a weak *Re* dependence when scaled on U_τ(see, e.g. Klewicki & Falco 1990; De Graaff & Eaton 2000; Metzger *et al.* 2001; Hoyas & Jiménez 2006; Hutchins & Marusic 2007; Vincenti *et al.* 2013). However, Monkewitz & Nagib (2015) argue that this inner peak cannot increase indefinitely with *Re*. In any case, the inner peak does not disappear with increasing *Re*. The data of Marusic *et al.* (2015) on a smooth wall turbulent boundary layer show convincingly that the inner peak remains even though the magnitude of $\overline{u^{+2}}$ increases in the outer layer, possibly leading to an outer peak which may eventually exceed the near-wall peak value. A similar behaviour is observed for the high *Re* ZPG TBL data of Fernholz & Finley (1996), Vincenti *et al.* (2013) and the high Reynolds number smooth wall pipe data of Morrison *et al.* (2004) and Hultmark *et al.* (2012). These latter authors attributed the occurrence of the outer peak to a shift in the production away from the wall when *Re* increases, supposedly resulting from an increasing separation between large and small scales.

The continuous evolution (in shape and magnitude) of the $\overline{u^{+2}}$ distribution with an ever increasing Reynolds number may be interpreted as reflecting the transient nature of the smooth wall TBL, and contrasts with that of a rough wall TBL. This can be seen in figure 8(*a*), where we have reported profiles of $\overline{u^{+2}}$ for the present 2-D rough wall at different Re_τ ranging from 620 to 7200, smooth wall data of Marusic *et al.* (2015) and the rough wall data of Squire *et al.* (2016). The data of Krogstad & Efros (2012) at $Re_\tau = 13\,300$ have also been included. Our measurements are consistent with those of Krogstad & Efros (2012) and Squire *et al.* (2016).

At low *Re*, profiles of $\overline{u^{+2}}$ on both the 2-D rod and sand-grain rough wall TBLs present a near-wall peak. Lee & Sung (2007), Lee *et al.* (2009) and Volino, Schultz & Flack (2011) respectively reported a similar inner peak in the low Reynolds number DNS, particle image velocimetry (PIV) and LDV measurements of a turbulent boundary layer over 2-D rough walls with a similar spacing $p = 8k$ as in the present case. As *Re* increases, this peak subsides while an outer layer peak appears. A similar behaviour of a decreasing inner peak was reported by Monty *et al.* (2010), who compared the turbulence statistics (obtained with matched l^+ values) over a range of *Re* in a turbulent boundary layer over a regular braille-type roughness. This behaviour is clearly evident in the Squire *et al.* (2016) data. These results confirm that the near-wall peak attenuation is not due to spatial resolution issues usually associated with hot-wire anemometry (see also the study of Hutchins *et al.* (2009)).

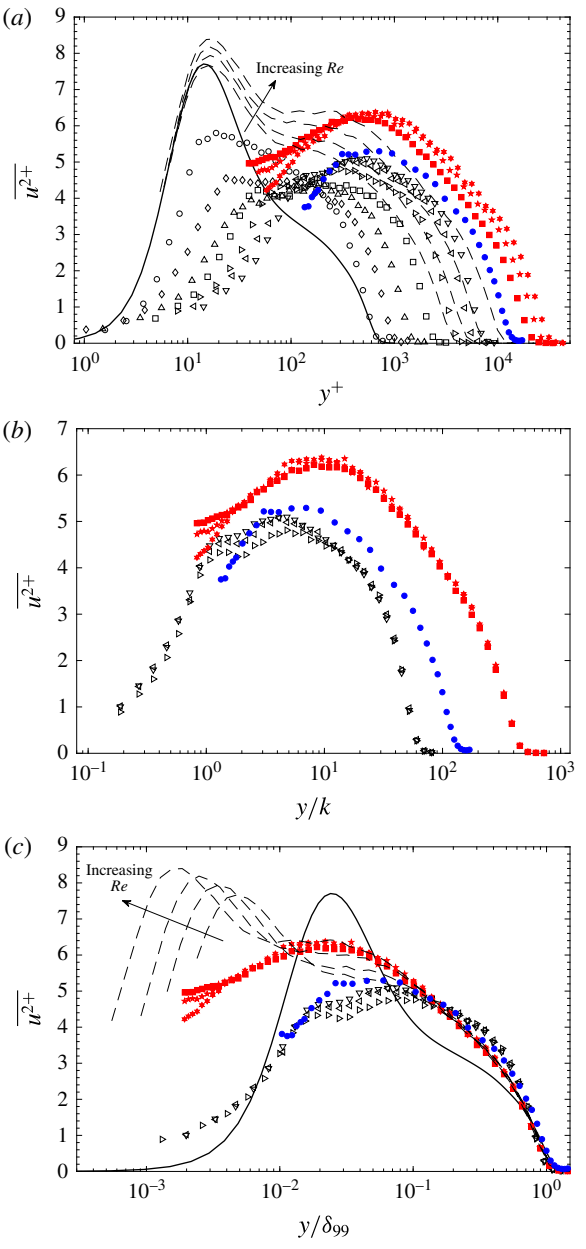

FIGURE 8. (Colour online) Profiles of $\overline{u^{+2}}$ in smooth and rough wall TBLs at several Re_τ as a function of (*a*) y^+; (*b*) y/k; and (*c*) y/δ. Smooth wall DNS (solid black line, $Re_\tau = 674$ Schlatter & Örlü 2010), smooth wall TBL (black dashed lines, $Re_\tau = 3370$, 4760, 6450 and 9830, Marusic *et al.* 2015), sand-grain roughness (red symbols, $Re_\tau =$ 20 160, 25 020 and 29 900, Squire *et al.* 2016), square bar (blue symbols, $Re_\tau = 13\,300$, Krogstad & Efros 2012) and the present rough wall data (black symbols). Refer to caption of figure 4 for symbols used for smooth wall, sand-grain and square bar rough wall TBLs.

The first five ($Re_\tau \leqslant 4000$) of our 2-D rod rough wall turbulence intensity profiles have l^+ values smaller than 20 (see table 1 for details). Looking at those five profiles, one can easily discern that the reduction in the magnitude of the inner peak as Re increases is due to roughness and not due to insufficient spatial resolution in our hot-wire measurements. Nonetheless, we realise that there is some spatial attenuation in our results particularly at high Re but emphasise that this does not affect the main conclusions of the paper. Squire *et al.* (2016) reached similar conclusions on the influence of l^+ on the inner peak. As the inner peak decreases, it also shifts towards larger y^+. Whilst it is not clear whether or not the inner peak is 'removed' or simply 'hidden' due to the large values of $\overline{u^{+2}}$ in the outer layer, the former scenario is expected because the near-wall region of the flow is entirely altered by the roughness at least when Re is sufficiently large and $4 \leqslant p/k \leqslant 16$ (e.g. Wang, Hejcik & Sunden 2007; Djenidi *et al.* 2008; Lee *et al.* 2009).

The horizontal shift is not limited to the inner peak. There is a clear systematic shift of the entire distribution of $\overline{u^{+2}}$, similar to that observed in the U^+ profiles, as Re_τ increases. However, the shape of the distributions seems to suggest a possible independence on Re of the $\overline{u^{+2}}$ profiles with increasing Re. This indicates that, like the mean velocity field, the fluctuating velocity field on the rough walls may comply with the Reynolds number similarity hypothesis. To ascertain this, we report in figure 8(*b*,*c*) some of the rough wall distributions of $\overline{u^{+2}}$ as functions of y/k and y/δ, respectively; these distributions correspond to the mean velocity profiles reported in figure 3. There is generally a good collapse for both sand-grain and 2-D rough wall boundary layers. For the present 2-D rough wall, the distribution for $Re_\tau = 3945$ deviates from the other two in the region $y/k \leqslant 10$, possibly reflecting a persistence of the transient state, which would indicate that the fluctuating velocity field is not yet 'fully' independent of Re. Just as in the case of normalised mean velocity profiles, the 2-D rough wall and the sand-grain rough wall have distinct Re-independent distributions of $\overline{u^{+2}}$.

4. Discussion and conclusions

Hot-wire measurements in a ZPG TBL layer over a 2-D rough wall with a separation between elements equal to $8k$ (k is the roughness element height) have been made to assess the behaviour of the TBL as the Reynolds number increases. The present results and those of Squire *et al.* (2016) on a sand-grain roughness are compared with those over a smooth wall. The comparison led to the following new observations:

(i) The downward shift on the mean velocity profile ΔU^+ on a rough wall reaches a limit as Re increases.

(ii) The limit for ΔU^+ depends on the roughness form drag.

(iii) The collapse of velocity defect profiles when normalised by the friction velocity between different surface conditions (smooth, 2-D roughness and sand-grain paper) does not indicate a Re-independent state.

(iv) The true indicator of Re-independent state is the collapse of the velocity defect profile when normalised by the friction velocity as Re increases.

(v) The scaling of the velocity defect with the free-stream velocity does not show a collapse between smooth and rough walls but also between rough walls with different roughness geometries.

The above observations lead to the following conclusions:

(i) A rough wall boundary layer quickly approaches a Re-independent state as indicated by the constancy of the ratio U_∞/U_τ (or C_f) with respect to Reynolds

number and the collapse of the normalised mean velocity and velocity variance profiles.

(ii) Different roughness geometries with different drag coefficients lead to different normalised mean velocity and velocity variance distributions. In each case, the distributions are *Re*-independent.

The above discussion suggests that a rough wall TBL can reach a *Re*-independent state at moderate Reynolds numbers when the roughness elements are such that the viscous drag is practically negligible in comparison to the form drag. This state is characterised by *Re*-independent normalised distributions for the mean velocity and the longitudinal Reynolds stress. However, these profiles are determined by the roughness geometry (i.e. C_f and/or the ratio δ/k) and thus, despite being *Re* independent, cannot in principle be universal in the sense that they all collapse onto the same distribution. However, a collapse should be observed for rough walls with identical C_f values. The existence of *Re*-independent state is intimately linked to self-preservation (Townsend 1956, 1976), which assumes that all normalised (or scaled) distributions of mean quantities (e.g. mean velocity and Reynolds stresses) have similar shape at all stages of development of the flow. Self-preservation requires only one set of velocity and length scales (all scaling velocities compliant with self-preservation must be proportional to each other; likewise for the scaling lengths).

Townsend (1956) showed that a TBL cannot be self-preserving over a smooth wall at finite *Re* because of the presence of a viscous dominated near-wall region, although the outer part of the boundary layer can evolve in a self-preserving manner. On the other hand, Talluru *et al.* (2016) showed that self-preservation can be achieved on a rough wall when k varies like x for any given (large enough) *Re*. This merits some discussion given that, for the present roughness, k is constant. Strictly, self-preservation cannot be achieved over the present rough wall, which consists of constant diameter rods. Yet, figure 9, which shows mean velocity profiles at several x positions in the smooth wall TBL (Marusic *et al.* 2015) and the present rough wall boundary layers, normalised by wall units, shows that there is relatively good collapse for the rough wall boundary layer over the streamwise fetch used in this study (see table 1). This indicates that U_τ remains approximately constant over that fetch. As expected, there is no collapse of the mean velocity profiles for the smooth wall boundary layer because U_τ continually varies with x (both U^+_{max} and δ^+ increases with x). These results are consistent with the self-preservation analysis of Talluru *et al.* (2016), who showed that one of the conditions for self-preservation is that U_τ must be constant along x. They also suggest that self-preservation can be achieved over a limited streamwise distance over which C_f remains approximately constant, even when the roughness height is not constant. The measurements of Squire *et al.* (2016) also confirm this. Indeed, their measurements cover a larger streamwise fetch, between 1.6 and 21.7 m at $U_\infty \simeq 20.4$ m s^{-1} (see table 2 of Squire *et al.* (2016)). In their study, U_τ decreases from $x \simeq 1.6$ m to $x \simeq 12$ m and then remains approximately constant for $x \geqslant 15$ m.

The reason why self-preservation is well approximated is associated with the fact that the spatially averaged mean velocity is not zero at the virtual origin, thus removing the no-slip condition and accordingly weakening significantly, if not removing, the viscous drag (the rough wall velocity profiles shown in figure 9 support this). This is also the condition for achieving a *Re*-independent flow, which is well observed in a fully rough wall TBL. A further comment is required regarding the removal of the no-slip condition. In the absence of this condition, there should be no boundary layer and no drag on a smooth wall. The classical laminar boundary

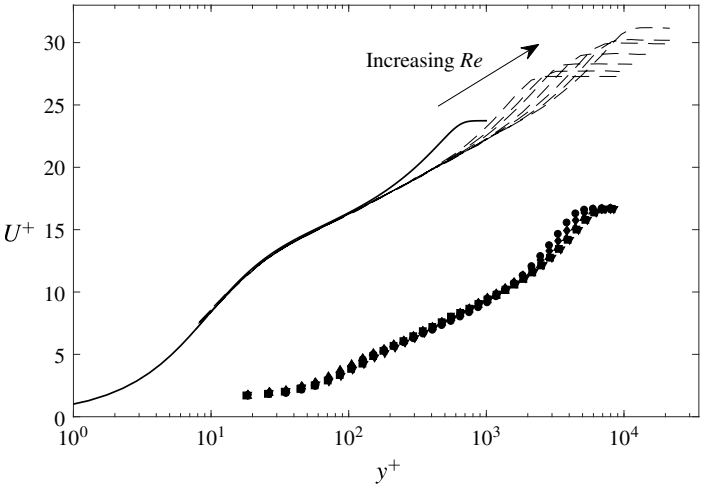

FIGURE 9. Mean velocity profiles at several streamwise locations on smooth and rough walls. Symbols: present rough wall measurements at $U_\infty \simeq 16$ m s^{-1} (see table 1 for symbols); dashed lines: smooth wall data at different x (cf. table 2 of Marusic *et al.* 2015, $Re_\tau = 2800$, 3600, 4300, 6000, 8400, 10 500 and 13 000) and solid line: smooth wall DNS data (Schlatter & Örlü 2010, $Re_\tau = 674$).

layer theory was developed by Prandtl aimed at accounting for the no-slip condition (which also causes a momentum deficit). On the rough wall, where the (spatially averaged) no-slip condition is removed, the roughness elements are the source of the drag and the momentum deficit, thus leading to the development of the boundary layer. In a fully rough regime, this boundary condition becomes consistent with self-preservation which vindicates Townsend's (1976) statement that 'if the motion around the roughness elements allows mean velocities and stresses of the self-preserving forms, self-preserving flow may be possible over the fully turbulent part of the flow'.

Acknowledgements

The authors acknowledge the Australian Research Council for its financial support. We thank Professor I. Marusic (University of Melbourne, Australia) and Professor P.-Å. Krogstad (Norwegian University of Science and Technology, Trondheim) for providing the statistics of a turbulent boundary layer over sand-grain and 2-D roughnesses, respectively.

REFERENCES

ALFREDSSON, P. H. & ÖRLÜ, R. 2010 The diagnostic plot – litmus test for wall bounded turbulence data. *Eur. J. Mech. (*B*/Fluids)* **29** (6), 403–406.

ALFREDSSON, P. H., ÖRLÜ, R. & SEGALINI, A. 2012 A new formulation for the streamwise turbulence intensity distribution in wall-bounded turbulent flows. *Eur. J. Mech. (*B*/Fluids)* **36**, 167–175.

ALFREDSSON, P. H., SEGALINI, A. & ÖRLÜ, R. 2011 A new scaling for the streamwise turbulence intensity in wall-bounded turbulent flows and what it tells us about the 'outer' peak. *Phys. Fluids* **23** (4), 041702.

AMIR, M. & CASTRO, I. P. 2011 Turbulence in rough-wall boundary layers: universality issues. *Exp. Fluids* **51** (2), 313–326.

ANTONIA, R. A. & DJENIDI, L. 2010 On the outer layer controversy for a turbulent boundary layer over a rough wall. In *IUTAM Symposium on the Physics of Wall-bounded Turbulent Flows on Rough Walls*, pp. 77–86. Springer.

BAARS, W. J., SQUIRE, D. T., TALLURU, K. M., ABBASSI, M. R., HUTCHINS, N. & MARUSIC, I. 2016 Wall-drag measurements of smooth-and rough-wall turbulent boundary layers using a floating element. *Exp. Fluids* **57** (5), 1–16.

BAKKEN, O. M., KROGSTAD, P.-Å., ASHRAFIAN, A. & ANDERSSON, H. I. 2005 Reynolds number effects in the outer layer of the turbulent flow in a channel with rough walls. *Phys. Fluids* **17** (6), 065101.

BHAGANAGAR, K., KIM, J. & COLEMAN, G. 2004 Effect of roughness on wall-bounded turbulence. *Flow Turbul. Combust.* **72** (2–4), 463–492.

CASTRO, I. P., SEGALINI, A. & ALFREDSSON, P. H. 2013 Outer-layer turbulence intensities in smooth- and rough-wall boundary layers. *J. Fluid Mech.* **727**, 119–131.

CHAUHAN, K. A., NAGIB, H. M. & MONKEWITZ, P. A. 2009 Criteria for assessing experiments in zero pressure gradient boundary layers. *Fluid Dyn. Res.* **41**, 021404.

DE GRAAFF, D. B. & EATON, J. K. 2000 Reynolds-number scaling of the flat-plate turbulent boundary layer. *J. Fluid Mech.* **422**, 319–346.

DJENIDI, L. & ANTONIA, R. A. 2012 A spectral chart method for estimating the mean turbulent kinetic energy dissipation rate. *Exp. Fluids* **53** (4), 1005–1013.

DJENIDI, L., ANTONIA, R. A., AMIELH, M. & ANSELMET, F. 2008 A turbulent boundary layer over a two-dimensional rough wall. *Exp. Fluids* **44** (1), 37–47.

FERNHOLZ, H. H. & FINLEY, P. J. 1996 The incompressible zero-pressure-gradient turbulent boundary layer: an assessment of the data. *Prog. Aeronaut. Sci.* **32** (4), 245–311.

FINNIGAN, J. 2000 Turbulence in plant canopies. *Annu. Rev. Fluid Mech.* **32** (1), 519–571.

FLACK, K. A., SCHULTZ, M. P. & SHAPIRO, T. A. 2005 Experimental support for Townsend's Reynolds number similarity hypothesis on rough walls. *Phys. Fluids* **17** (3), 035102.

GEORGE, W. K. 1989 The self-preservation of turbulent flows and its relation to initial conditions and coherent structures. *Advances in Turbulence*, pp. 39–73.

GEORGE, W. K. & CASTILLO, L. 1997 Zero-pressure-gradient turbulent boundary layer. *Appl. Mech. Rev.* **50** (12), 689–729.

HINZE, J. O. 1975 *Turbulence*. McGraw-Hill.

HOYAS, S. & JIMÉNEZ, J. 2006 Scaling of the velocity fluctuations in turbulent channels up to $Re_\tau = 2003$. *Phys. Fluids* **18** (1), 011702.

HULTMARK, M., VALLIKIVI, M., BAILEY, S. C. C. & SMITS, A. J. 2012 Turbulent pipe flow at extreme Reynolds numbers. *Phys. Rev. Lett.* **108** (9), 094501.

HUTCHINS, N. & MARUSIC, I. 2007 Evidence of very long meandering features in the logarithmic region of turbulent boundary layers. *J. Fluid Mech.* **579**, 1–28.

HUTCHINS, N., NICKELS, T. B., MARUSIC, I. & CHONG, M. S. 2009 Hot-wire spatial resolution issues in wall-bounded turbulence. *J. Fluid Mech.* **635**, 103–136.

JACKSON, P. S. 1981 On the displacement height in the logarithmic velocity profile. *J. Fluid Mech.* **111**, 15–25.

JIMÉNEZ, J. 2004 Turbulent flows over rough walls. *Annu. Rev. Fluid Mech.* **36**, 173–196.

JONES, M. B., NICKELS, T. B. & MARUSIC, I. 2008 On the asymptotic similarity of the zero-pressure-gradient turbulent boundary layer. *J. Fluid Mech.* **616**, 195–203.

KAMRUZZAMAN, M., DJENIDI, L., ANTONIA, R. A. & TALLURU, K. M. 2015 Drag of a turbulent boundary layer with transverse 2D circular rods on the wall. *Exp. Fluids* **56** (6), 1–8.

KLEWICKI, J. C. & FALCO, R. E. 1990 On accurately measuring statistics associated with small-scale structure in turbulent boundary layers using hot-wire probes. *J. Fluid Mech.* **219**, 119–142.

KROGSTAD, P.-Å. & ANTONIA, R. A. 1999 Surface roughness effects in turbulent boundary layers. *Exp. Fluids* **27** (5), 450–460.

KROGSTAD, P.-Å., ANTONIA, R. A. & BROWNE, L. W. B. 1992 Comparison between rough-and smooth-wall turbulent boundary layers. *J. Fluid Mech.* **245**, 599–617.

KROGSTAD, P.-Å. & EFROS, V. 2010 Rough wall skin friction measurements using a high resolution surface balance. *Intl J. Heat Fluid Flow* **31** (3), 429–433.

KROGSTAD, P.-Å. & EFROS, V. 2012 About turbulence statistics in the outer part of a boundary layer developing over two-dimensional surface roughness. *Phys. Fluids* **24** (7), 075112.

LEE, J. H., LEE, S. H., KIM, K. & SUNG, H. J. 2009 Structure of the turbulent boundary layer over a rod-roughened wall. *Intl J. Heat Fluid Flow* **30** (6), 1087–1098.

LEE, S. H. & SUNG, H. J. 2007 Direct numerical simulation of the turbulent boundary layer over a rod-roughened wall. *J. Fluid Mech.* **584**, 125–146.

LEONARDI, S., ORLANDI, P., DJENIDI, L. & ANTONIA, R. A. 2015 Heat transfer in a turbulent channel flow with square bars or circular rods on one wall. *J. Fluid Mech.* **776**, 512–530.

LEONARDI, S., ORLANDI, P., SMALLEY, R. J., DJENIDI, L. & ANTONIA, R. A. 2003 Direct numerical simulations of turbulent channel flow with transverse square bars on one wall. *J. Fluid Mech.* **491**, 229–238.

LIGRANI, P. M. & BRADSHAW, P. 1987 Spatial resolution and measurement of turbulence in the viscous sublayer using subminiature hot-wire probes. *Exp. Fluids* **5** (6), 407–417.

MARUSIC, I., CHAUHAN, K. A., KULANDAIVELU, V. & HUTCHINS, N. 2015 Evolution of zero-pressure-gradient boundary layers from different tripping conditions. *J. Fluid Mech.* **783**, 379–411.

MARUSIC, I., MCKEON, B. J., MONKEWITZ, P. A., NAGIB, H. M., SMITS, A. J. & SREENIVASAN, K. R. 2010 Wall-bounded turbulent flows at high Reynolds numbers: recent advances and key issues. *Phys. Fluids* **22** (6), 065103.

METZGER, M. M., KLEWICKI, J. C., BRADSHAW, K. L. & SADR, R. 2001 Scaling the near-wall axial turbulent stress in the zero pressure gradient boundary layer. *Phys. Fluids* **13**, 1819–1821.

MONKEWITZ, P. A. & NAGIB, H. M. 2015 Large-Reynolds-number asymptotics of the streamwise normal stress in zero-pressure-gradient turbulent boundary layers. *J. Fluid Mech.* **783**, 474–503.

MONTY, J. P., CHONG, M. S., MATHIS, R., HUTCHINS, N., MARUSIC, I. & ALLEN, J. J. 2010 A high Reynolds number turbulent boundary layer with regular 'Braille-type' roughness. In *IUTAM Symposium on the Physics of Wall-bounded Turbulent Flows on Rough Walls*, pp. 69–75. Springer.

MORRISON, J. F., MCKEON, B. J., JIANG, W. & SMITS, A. J. 2004 Scaling of the streamwise velocity component in turbulent pipe flow. *J. Fluid Mech.* **508**, 99–131.

NICKELS, T. B. 2010 *IUTAM Symposium on The Physics of Wall-Bounded Turbulent Flows on Rough Walls*. Springer.

ÖRLÜ, R., SEGALINI, A., KLEWICKI, J. & ALFREDSSON, P. H. 2016 High-order generalisation of the diagnostic scaling for turbulent boundary layers. *J. Turbul.* **17** (7), 664–677.

RAUPACH, M. R. 1981 Conditional statistics of Reynolds stress in rough-wall and smooth-wall turbulent boundary layers. *J. Fluid Mech.* **108**, 363–382.

ROTTA, J. C. 1962 Turbulent boundary layers in incompressible flow. *Prog. Aerosp. Sci.* **2** (1), 1–95.

SCHLATTER, P. & ÖRLÜ, R. 2010 Assessment of direct numerical simulation data of turbulent boundary layers. *J. Fluid Mech.* **659**, 116–126.

SMITS, A. J., MCKEON, B. J. & MARUSIC, I. 2011 High-Reynolds number wall turbulence. *Annu. Rev. Fluid Mech.* **43**, 353–375.

SQUIRE, D. T., MORRILL-WINTER, C., HUTCHINS, N., SCHULTZ, M. P., KLEWICKI, J. C. & MARUSIC, I. 2016 Comparison of turbulent boundary layers over smooth and rough surfaces up to high Reynolds numbers. *J. Fluid Mech.* **795**, 210–240.

TACHIE, M. F., BERGSTROM, D. J. & BALACHANDAR, R. 2000 Rough wall turbulent boundary layers in shallow open channel flow. *J. Fluids Engng* **122** (3), 533–541.

TALLURU, K. M., DJENIDI, L., KAMRUZZAMAN, M. & ANTONIA, R. A. 2016 Self-preservation in a zero pressure gradient rough wall turbulent boundary layer. *J. Fluid Mech.* **788**, 57–69.

TALLURU, K. M., KULANDAIVELU, V., HUTCHINS, N. & MARUSIC, I. 2014 A calibration technique to correct sensor drift issues in hot-wire anemometry. *Meas. Sci. Technol.* **25** (10), 105304.

TOWNSEND, A. A. 1956 *The Structure of Turbulent Shear Flow*. Cambridge University Press.

TOWNSEND, A. A. 1976 *The Structure of Turbulent Shear Flow*. Cambridge University Press.

VINCENTI, P., KLEWICKI, J., MORRILL-WINTER, C., WHITE, C. M. & WOSNIK, M. 2013 Streamwise velocity statistics in turbulent boundary layers that spatially develop to high Reynolds number. *Exp. Fluids* **54** (12), 1–13.

VOLINO, R. J., SCHULTZ, M. P. & FLACK, K. A. 2007 Turbulence structure in rough-and smooth-wall boundary layers. *J. Fluid Mech.* **592**, 263–293.

VOLINO, R. J., SCHULTZ, M. P. & FLACK, K. A. 2011 Turbulence structure in boundary layers over periodic two-and three-dimensional roughness. *J. Fluid Mech.* **676**, 172–190.

WANG, L., HEJCIK, J. & SUNDEN, B. 2007 PIV measurement of separated flow in a square channel with streamwise periodic ribs on one wall. *J. Fluids Engng* **129** (7), 834–841.

ZAGAROLA, M. V. & SMITS, A. J. 1998 Mean-flow scaling of turbulent pipe flow. *J. Fluid Mech.* **373**, 33–79.